Predictive and Measurement Methods for Delta Ferrite Determination in Stainless Steels

A chronological review from the first predictive diagram in 1920 up to the latest mathematical model is presented

BY M. ASUNCIÓN VALIENTE BERMEJO

ABSTRACT

Controlling the δ-ferrite content in stainless steels is of utmost importance as its content will influence the material properties and its on-site behavior in terms of weldability, corrosion resistance, toughness, and thermal stability. The δ-ferrite content can be determined by taking real measurements using magnetic or quantitative metallographic determination, or alternatively can be approached by using well-recognized predictive methods like the WRC-1992 diagram or the FNN-1999 artificial neural network, which are fed by the chemical composition of the weld deposit. This paper presents a chronological review from the first predictive diagram in 1920 up to the latest mathematical model, including also an overview of the different measurement methods available. The advantages, drawbacks, scope, and limitations of predictive and measurement methods are also outlined.

Introduction

The residual δ-ferrite that remains at room temperature once a stainless steel has been welded, that is, after it has experienced the process of melting followed by solidification, will determine the material's properties and behavior during its service lifetime. It is well known that primary ferritic solidification avoids the hot cracking phenomenon in austenitic stainless steels, but the determination of the solidification mode requires a metallographic analysis, which is a destructive test. Therefore, in practical terms, a minimum δ-ferrite content of 3–4 FN (Ferrite Number) is considered an acceptable indicator to ensure the absence of hot cracking during solidification. However, for specific applications or service conditions, it is necessary to impose a maximum δ-ferrite content; for example, for high-temperature conditions or thermal cycles (350°–900°C) when δ-ferrite can suffer from spinodal decomposition or be transformed into (σ) sigma-phase, causing embrittlement and a decrease in corrosion resistance. Chromium and molybdenum segregation enriches σ (sigma)-phase formed at the austenite/ferrite (γ/δ) grain boundaries, causing a depletion of these elements in the matrix and raising the material's vulnerability to corrosion. It is also necessary to establish a maximum δ-ferrite content in the case of stainless steels used under cryogenic conditions, as it influences the material's ductility and the low-temperature toughness. Some authors such as Brouwer (Ref. 1), and especially Lefebvre (Ref. 2), present detailed guides of the appropriate δ-ferrite contents according to the application for which the stainless steel is intended. In practical terms, the welding specifications included in fabrication contracts demand a level of δ-ferrite for welded assemblies. Therefore, the level of ferrite is a parameter to be measured by the quality assurance staff and its value should be set according to the risk that the welded material could experience a decrease in its properties.

The relationship between the δ-ferrite content, and the mechanical and corrosion-resisting properties in stainless steels, has encouraged researchers to discover predictive tools and measurement methods since the early part of the 20th century. Predictive methods are essential during the design stage of a project in order to have a good approach to the δ-ferrite level that will be achieved, when a weld deposit or pad is not available, or when different options of welding consumables are being considered.

When an experimental determination of δ-ferrite content is carried out, the literature (Refs. 1, 3–8) recognizes that within the same weld pad, local variations of δ-ferrite could be shown, due to compositional microsegregation related to variations in cooling conditions or also due to a loss of elements during the welding process. It is also recognized that for the same combination of base material and consumable, differences in the experimental values can also be found related to the specific welding procedure and parameters used. Therefore, whatever FN value is allocated to a weld metal should be derived from an average obtained from several measurements taken, as stated in the standard DIN 32514 (Ref. 5).

Presented below is a chronology of the different methods that researchers have proposed. It includes predictive and measurement methods. The advantages and drawbacks of the currently used methods are also considered.

KEYWORDS

Stainless Steels
δ-ferrite
Schaeffler Diagram
DeLong Diagram
WRC-1988 Diagram
WRC-1992 Diagram
Artificial Neural Network
FNN-1999
ORFN

Chronology of Predictive and Measurement Methods

Historically, authors have contributed to the literature with revisions and collections of the different methods used for the forecast and measurement of δ-ferrite in stainless steels. Worthy of notice is the revision carried out in 1986 by Stalmasek (Ref. 7), showing 25 documented ways to determine δ-ferrite, or the revisions written by Kotecki (Ref. 9) in 1997 and Lundin (Ref. 10) in 1999. In 1985, Olson (Ref. 11) presented a comprehensive review on methodology, starting at 1920 with Strauss

M. ASUNCIÓN VALIENTE BERMEJO (valiente.asun@gmail.com) *is an independent researcher and consultant, Barcelona, Spain.*

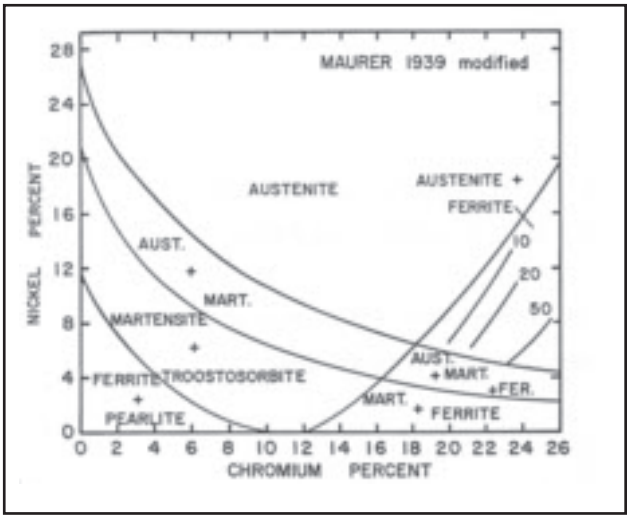

Fig. 1 — Maurer diagram, 1939 version. Composition range: Cr (0–26%) and Ni (0–25%) (Ref. 11).

and Maurer who introduced a diagram Cr vs. Ni to forecast the metallographic phases in rolled stainless steels. Figure 1 shows the later modification that Maurer made to the initial diagram. From that date, World War II was the motivation for studies on the development of Cr-Ni compositions for dissimilar welds in military armour, which led researchers to focus on expressions to correlate the chemical composition of alloys with suitable stability between δ-ferrite and γ-austenite phases. According to that, in 1938 Newell and Fleischman established a mathematical equation (Equation 1) to describe the boundary between austenitic microstructure and a (γ-austenite + δ-ferrite) mixed microstructure.

$$Ni = \frac{\left(Cr + 2Mo - 16\right)^2}{12} - \frac{Mn}{2} + 30\left(0.10 - C\right) + 8 \qquad (1)$$

In 1943, Field, Bloom, and Linnert (Equation 2); Binder, Brown, and Franks in 1949; and Thomas, also in 1949 (Equation 3), proposed similar equations to establish the boundary between austenite stability and the formation of δ-ferrite, but grouping in the same arm of the expression all the alloying elements that promoted the same microstructural phase.

$$Ni + 0.5Mn + 30C = \frac{\left(Cr + 2Mo - 16\right)^2}{12} + 14 \qquad (2)$$

$$Ni + 0.5Mn + 30C = 1.1(Cr + Mo + 1.5Si + 0.5Nb) - 8.2 \qquad (3)$$

The next natural step was taken in 1946 by Campbell and Thomas who proposed the concept of *chromium equivalent* for the first time during the microstructual study of welded alloy 25Cr-20Ni while adding small quantities of molybdenum and niobium. The concept of equivalent included the contribution of those alloying elements responsible for the specific phase formation, as depicted in Equation 4.

$$Cr_{eq} = Cr + 1.5Mo + 2Nb \qquad (4)$$

These initial researches, based on the linearized contribution of the alloying elements to the microstructure, were the basis for the next δ-ferrite predictive diagrams that were developed prior to 2000, when complex neural networks based on nonlinear regressions emerged.

In 1947, Schaeffler published his first diagram (Fig. 2A), which presented his first expressions for chromium and nickel equivalents in the axes (Equation 5) and plotted the microstructual phases observed.

$$\left.\begin{aligned} Cr_{eq} &= Cr + 1.8Mo + 2.5Si + 2Nb \\ Ni_{eq} &= Ni + 0.5Mn + 30C \end{aligned}\right\} \qquad (5)$$

As shown in the diagram, the microstructural boundary between γ-austenite and the two phases (δ-ferrite + γ-austenite) is claimed to follow a second-degree expression (Equation 6).

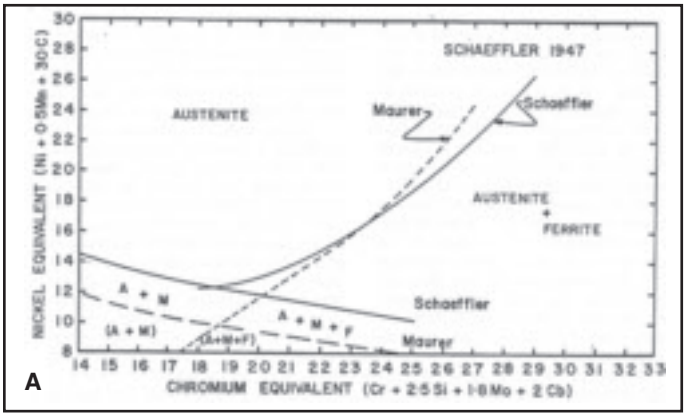

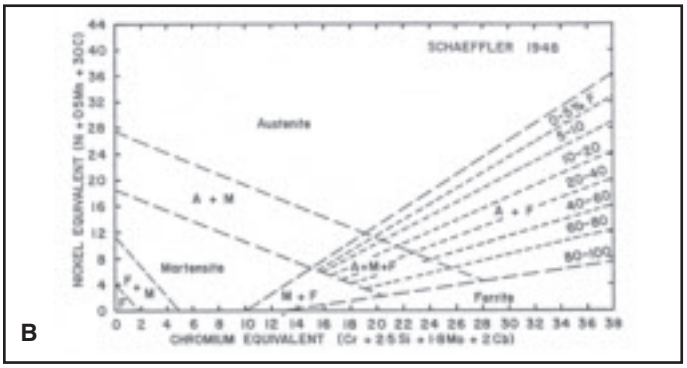

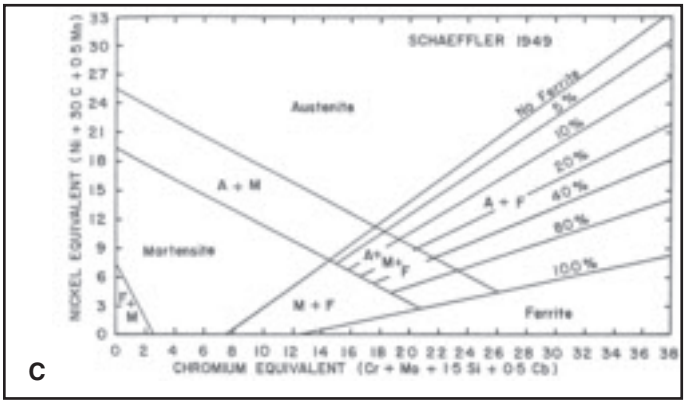

Fig. 2 — The various Schaeffler diagrams. A — 1947 version; B — 1948 version (Ref. 11); C — 1949 definitive version (Ref. 13).

$$Ni_{eq} = 12 + \frac{\left(Cr_{eq} - 16\right)^2}{12} \qquad (6)$$

In 1948, Schaeffler published a revised diagram (Fig. 2B) with iso-ferrite lines expressed as % ferrite (Ref. 12), which had been determined by quantitative metallography, and eventually, in 1949, the currently known Schaeffler diagram was presented (Ref. 13) (Fig. 2C). The expression for the chromium equivalent calculation (Equation 7) was changed, decreasing the relative weight of molybdenum, silicon, and niobium compared with the equivalent initially proposed (Equation 5). However, the microstructural phases observed and the %-vol ferrite were still shown.

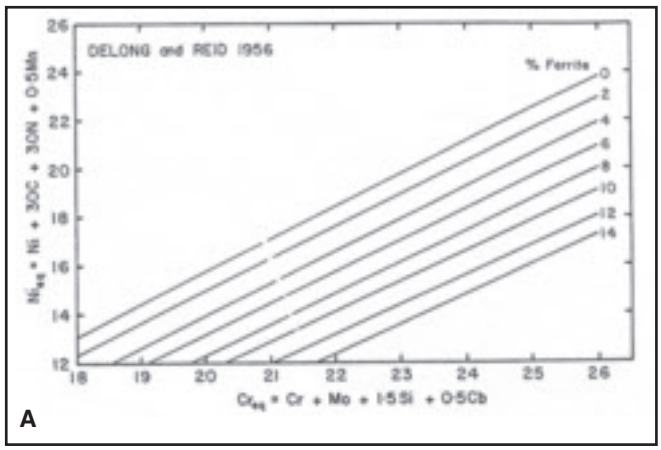

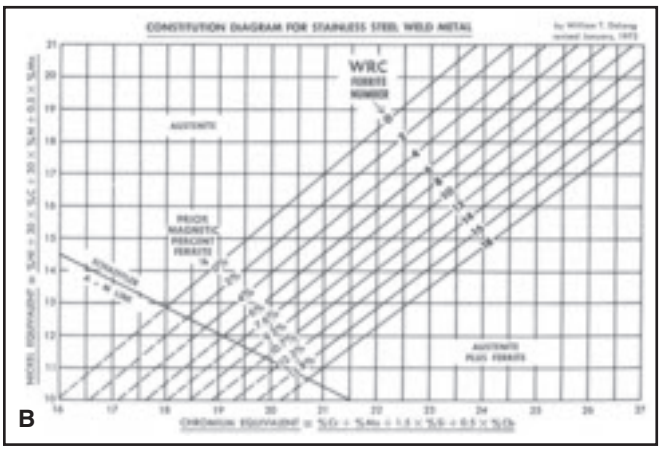

Fig. 3 — The DeLong diagrams. A — 1956 version (Ref. 11); B — 1973 definitive version (Ref. 15).

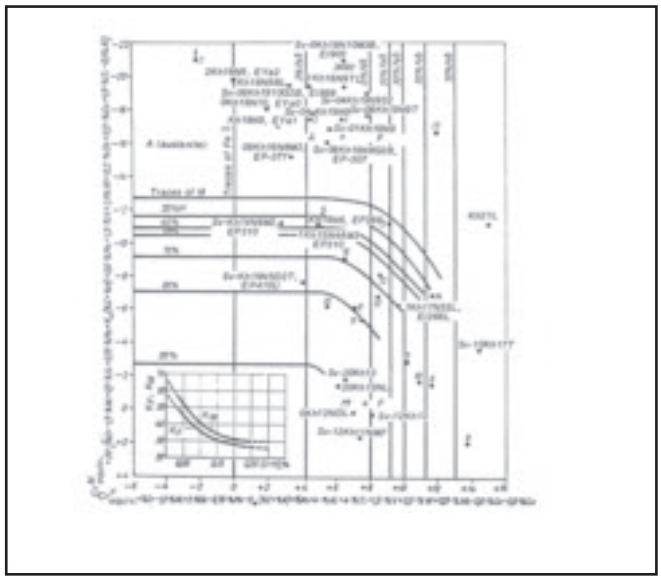

Fig. 4 — Potak diagram (Ref. 18). Compositional application range of the diagram: Cr, 10–22%; Ni, <10%; C and N, 0.03–0.20%.

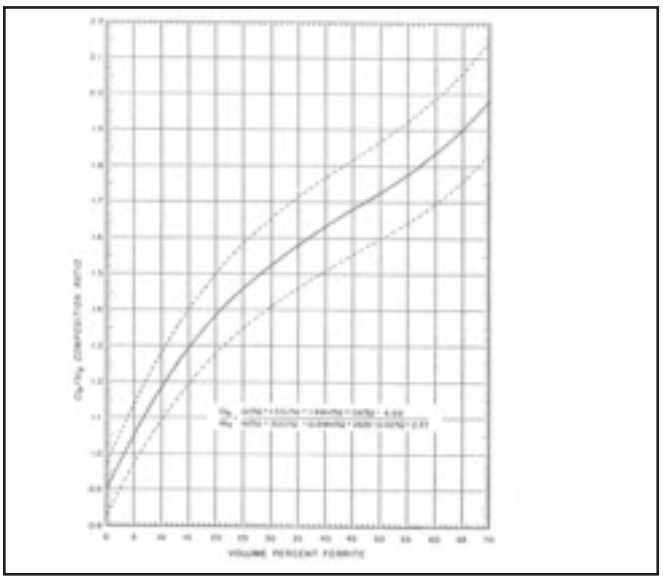

Fig. 5 — Schoefer diagram (Ref. 20). Cr, 17–28%; Ni, 4–13%; Mo, 0–4%; Nb, 0–1%; and up to 0.20% C, 0.20% N, 2% Mn, and 2% Si.

$$Cr_{eq} = Cr + Mo + 1.5Si + 0.5Nb \qquad (7)$$

This diagram was claimed to give a global precision of ± 4%-vol ferrite, or ± 3 FN for 78% of cases, and it has been extensively used for ferrite prediction in welded stainless steels and for microstructure prediction in dissimilar welds once the characteristic percentage dilution due to the welding process is known.

In 1956, DeLong (Refs. 14–17) expanded the austenite-ferrite transition area of Schaeffler's diagram and established the first version of his diagram — Fig. 3A. DeLong studied the influence of the nitrogen on the reduction of δ-ferrite content observed in the weld metal due to the entrance of this element into the weld pool because of turbulence in the gas flow in GMAW and GTAW or due to an excessive arc length in SMAW. He quantified the austenitizing effect of the nitrogen with a coefficient of 30 (like carbon) in the expression of nickel equivalent, while he considered valid the last Schaeffler's expression for chromium equivalent (Equation 8). DeLong also modified the location of the iso-ferrite lines of Schaeffler in order to improve the diagram's precision for new higher alloyed austenitic materials (AISI 309, 316, 317), and he used magnetic determination instead of metallographic determination in his first diagram. It was claimed that diagram presented a global precision of ± 3%-vol ferrite for 92% of cases, improving the predictions made by Schaeffler's diagram for austenitic stainless steels. DeLong based his first diagram on the results obtained from the preparation of around 600 as-welded samples prepared by SMAW.

$$\left.\begin{aligned} Cr_{eq} &= Cr + Mo + 1.5Si + 0.5Nb \\ Ni_{eq} &= Ni + 0.5Mn + 30C + 30N \end{aligned}\right\} \qquad (8)$$

In 1973, DeLong presented a revision of his first diagram (Ref. 15) (Fig. 3B). The main innovation was the presence of two ferrite scales, as it included the previous %-vol iso-ferrite lines and also incorporated the Ferrite Number (FN), which was the new scale the Welding Research Council (WRC) standardized. Ferrite Number will be explained in more detail later. DeLong also complemented the diagram with new experimental results from GTAW and GMAW weld pads in order to replace the ancient extrapolations he had established for ferrite contents higher than 8 FN; therefore, changes in the slopes of the iso-ferrite lines were carried out to improve the ferrite prediction of higher alloyed stainless. For 95% of cases, precision was claimed to be ± 3 FN for GMAW and GTAW and ± 4 FN for SMAW.

Parallel to research on welding, other authors, in particular Potak (Ref. 18) in 1972 and Schoefer (Ref. 19) in 1974, established their own Cr_{eq} and Ni_{eq} coefficients and developed diagrams for microstructural prediction including δ-ferrite content in the specific case of stainless steel castings. Figure 4 shows the Potak diagram, which includes both Cr_{eq}^{M} and Cr_{eq}^{F} equivalents

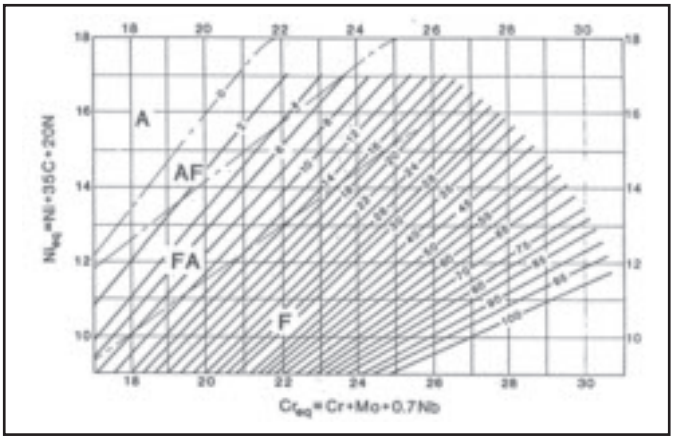

Fig. 6 — WRC-1988 diagram (Ref. 30). Better precision when the composition range is between the following: Cr_{eq}: 17–30%, Ni_{eq}: 9–17%, and Mn <10%, Mo <3%, N <0.2%, Si<1%.

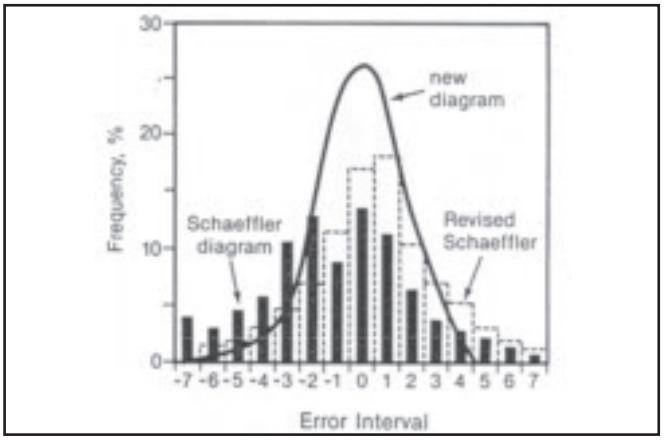

Fig. 7 — Comparative histograms: WRC-1988/DeLong/Schaeffler (Ref. 31). Note: "new diagram" refers to WRC-1988 and "revised Schaeffler" refers to DeLong's.

representing the influence of alloying elements in the formation of martensite and ferrite, respectively. Figure 5 shows the Schoefer diagram for castings, where dashed lines show the error interval. ASTM Standard A800-1991 (Ref. 20) recognizes the method for δ–ferrite prediction in stainless steel castings.

Until 1973, the main technique for the experimental determination of δ-ferrite content was based on metallography. The sample was etched by a reagent to reveal contrast between δ-ferrite and γ-austenite phases and a grid was superimposed over the image obtained by microscopy to determine by point-counting the percentage of δ-ferrite in the sample. The limitations of this technique will be mentioned later. During the same period, magnetic methods for the experimental determination of δ-ferrite appeared, based on the ferromagnetic response of the δ-ferrite over the paramagnetism of austenite.

Schaeffler in 1949 and Delong in 1956 presented the δ-ferrite content in their diagrams in terms of %-vol of δ-ferrite. However, at that time there was a serious problem in terms of the experimental reproducibility because every laboratory could use its own metallographic reagent with different phase-contrast capacity, or alternatively whatever magnetic equipment could be used. Consequently, when the δ-ferrite content was measured, a wide variability and dispersion of results was reported from different laboratories carrying out the test.

The WRC, the International Institute of Welding (IIW), and other researchers such as Björkroth (Ref. 21) stated the need to establish a standard for the determination of δ-ferrite content in stainless steels. In this way, the WRC with the IIW established a procedure in 1972 for the standardization of δ-ferrite measurements. The arbitrary term Ferrite Number was defined according to the attractive force between a standard magnet and a set of primary standards made of mild steel substrate electroplated with different thicknesses of nonmagnetic coating. The procedure defined the relationship between FN and the primary standards and it also established a series of secondary calibration standards to be used when magnetic measurement equipment cannot be calibrated with primary standards. Soon afterward, in 1974, the American Welding Society (AWS) published this procedure as the standard AWS A4.2 (Ref. 22), and later it was adopted also as ISO 8249 (Ref. 23). All the specific details related to the standards and the procedure can be found in the bibliography (Refs. 7, 9).

From that historical moment, DeLong updated his diagram in 1973 to the new FN scale, and since then researchers and industry have tended to limit the use of the % ferrite scale because of the absence of a reference standard and the lack of agreement in its quantification procedure.

Between 1973 and 1988, researchers such as Hull (Ref. 24) and Kotecki (Refs. 25–27) studied the effect of certain alloying elements on the level of δ-ferrite and proposed new coefficients for some elements in the chromium and nickel equivalents. Specifically, Hull proposed new chromium and nickel equivalents (Equation 9), adding the contribution of some minor alloying elements on the Schaeffler diagram and proposing a second-degree contribution for manganese on the nickel equivalent. Kotecki studied the influence of molybdenum, manganese, and silicon and proposed corrections for the DeLong coefficients (Equation 8), reducing the molybdenum coefficient in the Cr_{eq} from 1 to 0.7, and regarding manganese a constant value of 0.35 in the DeLong Ni_{eq}. This was suggested because in those alloys with concentrations higher than 2.5% Mn, DeLong seemed to underestimate the FN value. Regarding silicon, Kotecki considered that the coefficient of 1.5 proposed by Schaeffler and DeLong overestimated the effect of this element, and he suggested a coefficient close to 0.1. However, some years later in 1992, Kotecki did not include any coefficient for silicon nor for manganese and he returned to the unitary coefficient for molybdenum in his new diagram.

$$\left\{\begin{array}{l} Ni_{eq} = Ni + 0.11Mn - 0.0086Mn^2 + 18.4N \\ \quad +24.5C + 0.41Co + 0.44Cu \\ Cr_{eq} = Cr + 1.21Mo + 0.48Si + 2.27V + 0.72W \\ \quad +2.20Ti + 0.14Nb + 0.21Ta + 2.48Al \end{array}\right\} \quad (9)$$

In 1982, Kotecki (Refs. 28, 29) solved a new practical problem that emerged from the arrival in the market of a new group of stainless steels, the duplex types, with contents of approximately 50%-vol δ-ferrite. The previously established standard the WRC promoted and the AWS adopted in 1974 only allowed measurements up to 28 FN, due to the available equipment and the established calibration standards. Using a counterweight with Magne-Gage equipment and a wider range of primary standards, Kotecki managed to measure ferrite contents up to 100 FN. The WRC and AWS accepted this methodology, and consequently, the revised AWS A4.2-86 and the first edition of ISO 8249-1985 added the calibration standards to cover the whole measurement range including duplex stainless steels.

In 1988, Siewert, McCowan, and Olson (Ref. 30) developed a new diagram for the prediction of δ-ferrite content using a system of multivariable linear regressions where FN was the dependent variable and every alloying element was an independent variable. With the help of software, they optimized the linear regressions with an iterative process until the diagram was complete. The input data used to develop the linear regressions belonged to the WRC database (Ref. 31), which includes

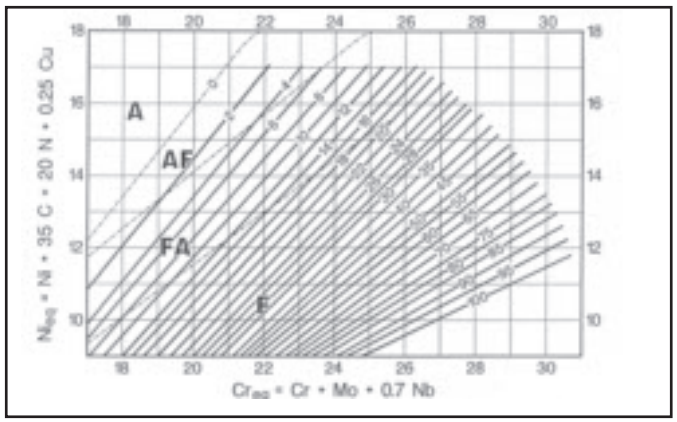

Fig. 8 — WRC-1992 diagram (Ref. 32). Compositional limits: Cr_{eq}, 17–31%; Ni_{eq}, 9–18%.

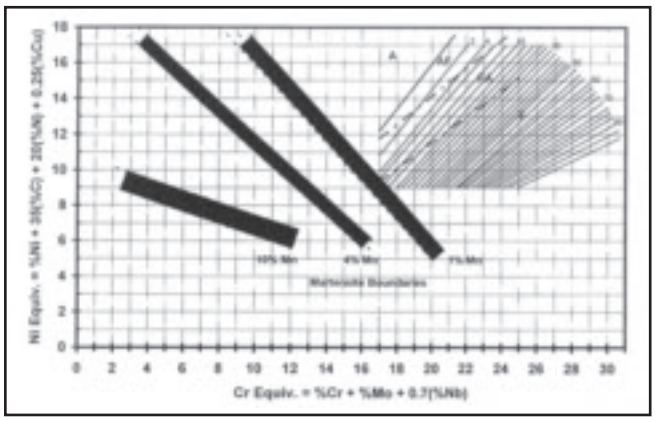

Fig. 9 — WRC-1992 diagram with martensite boundaries for 1, 4, and 10% Mn (Ref. 35).

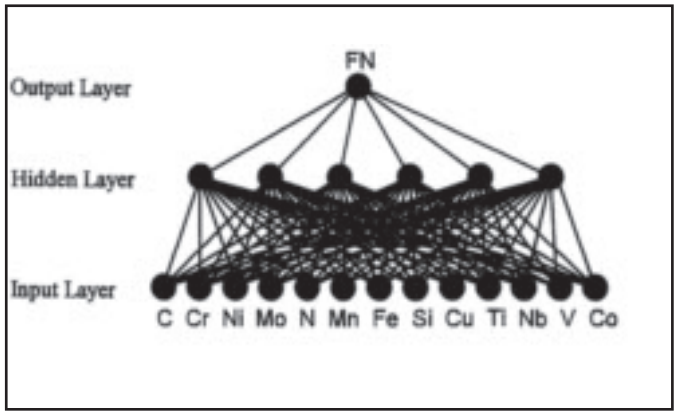

Fig. 10 — FNN-1999 artificial neural network sketch (Ref. 42).

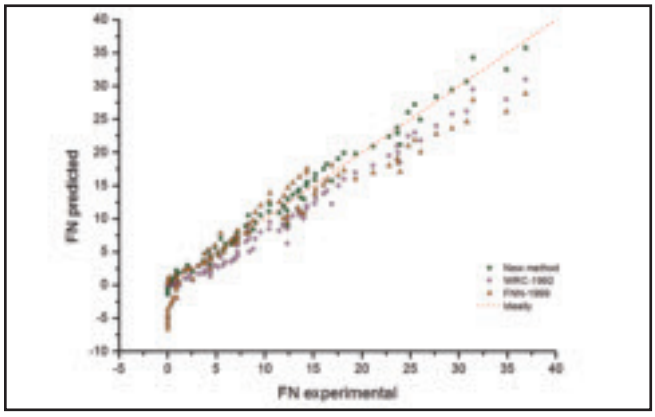

Fig. 11 — Comparison among forecast methods: New model, WRC-1992 diagram, and FNN-1999 neural network (Ref. 47).

the chemical composition and the FN value of 923 stainless alloys. Unlike DeLong's diagram, which was only based on AISI-300 austenitic stainless steels, this new diagram also included data for higher alloyed austenitics, duplex and other experimental alloys, increasing the prediction range up to 100 FN. Other important differences from former diagrams were the representation of the solidification modes (A, AF, FA, F) instead of the metallographic phases, and the fact that it included the lines or boundaries between the different solidification modes. The diagram was designated as WRC-1988 (Fig. 6) and the chromium and nickel equivalents proposed by the authors are shown in Equation 10.

$$\left\{\begin{array}{l} Ni_{eq} = Ni + 35C + 20N \\ Cr_{eq} = Cr + Mo + 0.7Nb \end{array}\right\} \qquad (10)$$

The predictions made with the WRC-1988 diagram were compared with those made with the Schaeffler and DeLong diagrams for the samples collected in the WRC database (Ref. 31). In order to establish a fair comparison with DeLong, only data with FN<18 were considered, since DeLong's diagram was not designed for higher δ-ferrite content alloys. It was claimed that the WRC-1988 predicted 84% of cases with an error better than ± 2.5 FN, while DeLong predicted only 66% of cases with this same level of error. Establishing the comparison with Schaeffler's diagram, for samples with FN>18, it was claimed that only 35% of cases would have an error better than ± 9 FN and for samples with FN<18, 52% of cases would have an error in the range of ± 2.5 FN. It was stated that DeLong's diagram presented an improvement compared with Schaeffler's, but it was also clear that the WRC-1988 diagram improved DeLong's. In order to illustrate these differences between the diagrams' accuracy, Fig. 7 shows the corresponding histograms. Checking the WRC-1988 goodness-of-fit using compositions and experimental FNs different from the WRC database, it was claimed that for data up to 35 FN, the diagram showed an error of ± 4 FN for 95% of samples (confidence interval 2σ) and for samples with FN > 35, the error could reach up to ± 10 FN for 95% of samples.

In 1992, Kotecki and Siewert (Refs. 32, 33) made a modification to the WRC-1988 diagram, adding a coefficient for copper in the nickel equivalent (Fig. 8 and Equation 11) in order to improve the accuracy of the FN prediction in those duplex stainless steels containing around 2% Cu. The extension of the axes — in Schaeffler's style — was also considered, and the new diagram, known as the WRC-1992 diagram, was designed to be used for predicting chemical compositions and FN values for welds or claddings on dissimilar materials, according to the percentage dilution occurring in the procedure.

$$\left\{\begin{array}{l} Ni_{eq} = Ni + 35C + 20N + 0.25Cu \\ Cr_{eq} = Cr + Mo + 0.7Nb \end{array}\right\} \qquad (11)$$

In 1994, this WRC-1992 diagram replaced DeLong's diagram in the ASME III code, and it is still considered valid for austenitic and duplex stainless steels.

Later, in 1999, Kotecki (Refs. 34, 35) increased the application of the WRC-1992 diagram for stainless steel claddings with 1, 4, and 10% manganese, whereby the influence of manganese on the martensite boundaries was included on the same WRC-1992 diagram — Fig. 9. Since Schaeffler's diagram, nobody had published work on the limits of martensite

formation until Kotecki did so.

The last of these diagrams was developed in 2000 by Balmforth and Lippold (Ref. 36) in order to represent the microstructures and the % ferrite in ferritic and martensitic stainless steels. In this case, as both martensite and ferrite have magnetic response, it was necessary to carry out a metallographic analysis to distinguish each phase and the iso-ferrite lines are expressed as % ferrite.

From the end of the 1990s until today, innovations related to the prediction of ferrite content in stainless steels have accompanied development of powerful computer software. Examples include the Aström regression (Ref. 37) (Equation 12) or Kannan regression (Ref. 38) (Equation 13) for the prediction of FN in FCAW claddings of duplex, based on welding parameter settings. Also worthy of mention is the research carried out in 2007 by Anderson et al. (Ref. 39) regarding the influence of molybdenum on the ferrite content of stainless steel welds.

$$FN = -48.53 - 13.85\,C + 12.73\,Si + 1.16\,Mn + 3.89Cr - 3.14\,Ni + 4.60\,Mo + 10.10\,Cu - 20.36\,N \quad (12)$$

$$\left\{\begin{array}{l} FN = 31.596 - 3.750I - 4.333S + 1.000N \\ -1.750T + 0.771I^2 - 1.479S^2 + 0.521N^2 \\ +1.375IT - 2.000ST \\ \text{I = Welding current } (A) \\ S = \text{Welding speed } (cm/min) \\ N = \text{Distance from the tip of the torch to the surface } (mm) \\ T = \text{Torch angle } (degrees) \end{array}\right. \quad (13)$$

However, in the 21st Century, a significant advancement in the prediction of FN has been the development of artificial neural networks, which have also been used to establish relationships between the chemical composition of the materials and some physical properties. For example, Bhadeshia et al. (Ref. 40) proposed neural networks for the prediction of fatigue crack growth and creep rupture. In the case of FN prediction, Vasudevan et al. (Ref. 41) and Vitek et al. (Refs. 42–45) have developed neural networks based on the chemical composition of austenitic and duplex stainless steels using the WRC database (Ref. 31) as input data.

The artificial neural network is a multivariable nonlinear regression method that can identify complex relationships between variables that are difficult to recognize by linear regression. The method is based on the interaction between three layers, as shown in Fig. 10. The first layer is constituted of input nodes representing the concentration of each alloying element; in the case of Vitek's network, it is formed by 13 elements. Secondly, there is a hidden layer with an adjustable number of nodes that have to be optimized in order to get the best forecast in the result but without overloading the system of variables. For Vitek's network, this is achieved with six hidden nodes. The third layer is the output layer containing one single node whose value is the predicted FN value.

Vitek recognized that the residual δ-ferrite content at room temperature depends on different variables that are interconnected, such as the chemical composition, the solidification mode, and the cooling rate, which in turn control the solid-state transformation δ→γ. Therefore, Vitek stated that the chromium and nickel equivalent expressions, which consider the influence of every alloying element as a constant throughout all the composition ranges and which do not consider a possible interaction between the alloying elements, are a very simplified way to deal with the subject.

Vitek developed two neural networks between 2000 and 2003, the FNN-1999, which only considered the chemical compositions as input data, and the ORFN, which added the weld cooling rate to the previously mentioned parameters.

To develop the ORFN neural network, Vitek used cooling rate data from different sources. He used the WRC database, which includes compositional data from arc welding samples but not cooling rates, and he considered taking a constant value of 10°C/s for all those samples. For the new welds he prepared with the laser beam welding process, due to the small dimensions of the sample, in some cases he could not use magnetic methods for the δ-ferrite determination and had to use quantitative metallography, while in other cases, he used some mathematical expressions given in the bibliography. However, it was found to be difficult to consolidate the cooling rate data originating from different sources, so cooling rate data were given within an order of magnitude.

Vitek's ORFN neural network application range is between the following: 10–3.10^6 °C/s, 0–131 FN, 14.7–32% Cr, 4.6–33.5% Ni, 0.008–0.2% C, 0.01–6.85% Mo, 0.35–12.7% Mn, 0.003–1.3% Si. According to Vitek's study, the FNN-1999 neural network is claimed to make a more accurate prediction than the WRC-1992 diagram and the ORFN neural network. However, in the case of laser or high-energy processes, which are related to high cooling rates, it is claimed the ORFN neural network makes the most accurate predictions.

In 2010, the author of this paper presented a new method for forecasting FN in austenitic stainless steels under arc electric solidification conditions (Refs. 46, 47). That work led to the conclusion that FN depends on two variables: the total allowing level (Cr_{eq}+Ni_{eq}) and the ratio Cr_{eq}/Ni_{eq}. By using Hammar and Svensson's equivalents (Ref. 48) (Equation 14), a general expression was proposed (Equation 15).

$$\left\{\begin{array}{l} Cr_{eq} = Cr + 1.37Mo \\ Ni_{eq} = Ni + 0.31Mn + 22C + 14.2N \end{array}\right\} \quad (14)$$

$$FN = 54.22 - 126.26\left(Cr_{eq} + Ni_{eq}\right) + \left[-48.11 + 37.14\left(Cr_{eq} + Ni_{eq}\right)\right]\left(\frac{Cr_{eq}}{Ni_{eq}}\right) + \left[-0.23 + 61.95\left(Cr_{eq} + Ni_{eq}\right)\right]\left(\frac{Cr_{eq}}{Ni_{eq}}\right)^2 \quad (15)$$

In order to validate the new general expression (Equation 15), the WRC database (Ref. 31), which contains 279 samples whose chemical compositions are within the range of the austenitics, was used. Therefore, the Cr_{eq} and Ni_{eq} were calculated from the chemical composition provided by the database and then the (Cr_{eq} +Ni_{eq}) and (Cr_{eq}/Ni_{eq}) values were calculated for each sample and introduced in Equation 15 in order to obtain a predicted FN value. The predicted FN values were then compared with the experimental FN provided by the database. Statistical processing confirms that the expected error is + 1.01 with a ± 1.06 FN confidence interval for a probability of 68% and a ± 2.12 FN confidence interval for a probability of 95%. Therefore, the general expression provides FN estimation with an error of 1.01 FN ± 2.12 FN and a probability of 95%.

The level of error given by Equation 15 could be compared with the DeLong and WRC-1988 histogram shown in Fig. 7. As shown there, for the FN range between 0 and 18, DeLong's histogram is centered at an error of +2 FN with a ± 8 FN confidence interval, and for the same FN range, the WRC-1988 is centered at –1 FN with a ± 4 FN for a confidence interval of 95%. These are higher errors than those obtained with the general expression in Equation 15.

As has been demonstrated, the most accurate methods for forecasting FN in arc welding were the WRC-1992 diagram and the FNN-1999 neural network. Therefore, to compare the accuracy and good fit between those methods and the new Equation 15, the chemical composition of the 87 samples prepared in the research were used as input data for the three methods and the results are depicted in Fig. 11. The dotted red line represents the ideal 1:1 trend, where the experimental

and the calculated FN values match. The rose circles represent the correlation between the experimental FN and the FN predicted with the WRC-1992 diagram, while the orange triangles refer to the FNN-1999 neural network and the green squares represent the correlation of the general expression Equation 15. It is shown that the WRC-1992 underestimates the FN value throughout all the composition ranges while the FNN-1999 makes an accurate forecast for samples with FN<10. However, similar to WRC-1992, that method also underestimates the values for samples with FN>15. It is clear that the general expression provides better matches than do WRC-1992 and FNN-1999 for these 87 samples.

Current Methods for Measurement and Prediction of δ-Ferrite: Scope and Limitations

This section presents the scope and limitations of the currently used measurement techniques and predictive methods.

Predictive Methods

Predictive methods have their scope and application in those cases where the project is in a preliminary study stage where the weld pad is not yet available, or when different alternatives of welding consumables are under consideration and obtaining an estimate of the δ-ferrite content is of importance. Well-known construction codes like ASME Section III have accepted the accuracy of the predictive methods and, consequently, the use of such methods is demanded in some nuclear procedures and fabrication contracts.

Currently, the WRC-1992 diagram is still the most used method in the industry, but as has been shown in the previous section, the neural networks and the recent new method (Equation 15) for austenitics have demonstrated higher accuracy.

Prediction diagrams need the input of the chemical composition of the weld metal whose δ-ferrite content is going to be predicted. In general terms, the accuracy of the chemical composition entered determines the accuracy given by the diagrams. Low accuracy in the composition or the use of consumable composition instead of weld metal composition would imply more inaccuracy in the prediction. It should be noted that each diagram has been obtained according to specific assumptions in terms of linear regressions, and that variations in the chemical composition could also be attributed to the specific welding process and its settings. For example, the chromium content can change in SAW depending on the specific flux used, or in SMAW, GTAW, or GMAW the atmospheric nitrogen could be absorbed into the weld pool if the arc length is too long. Moreover, diagrams also have another limitation, which is the fact that the influence of the cooling rate on the residual δ-ferrite is not considered, and they have been developed only to be used under electric arc conditions. Regarding this point, some studies (Refs. 49–52) confirm that the conventional diagrams proposed by Schaeffler, DeLong, and for WRC-1992, are not suitable for use under the range of cooling rates associated with high-energy welding processes like laser beam (LBW) or electron beam (EBW), and consequently, the estimation of the δ-ferrite content obtained from the diagrams would not be correct under those conditions. Some researchers (Refs. 50, 52, 53) have proposed modifications of the traditional Schaeffler diagram in order to adapt it to higher cooling rate conditions, but these modifications have their limitations.

Regarding the limitation of artificial neural networks, it comes from the accuracy and the size of the database used for training the network, as well as from the inner architecture of the net that needs to be optimized. The FNN-1999 neural network was generated from the same database as the WRC-1992 diagram; therefore, it does not take into consideration the effects of cooling rate, and it is only recommended for FN prediction of arc welds. Regarding the ORFN neural network, difficulties with the consolidation of cooling rates have been described, but the method can be used to forecast FN for arc welding and laser beam welding.

Finally, the recently presented expression (Equation 15) is only valid for austenitic stainless steel arc welds.

Measurement Methods

There are several different techniques for the measurement and determination of δ-ferrite; however, magnetic determination is the most extensively used in the industry because it is nondestructive and provides an immediate result. This section describes the scope and limitation of the different techniques currently used.

Magnetic Determination

The WRC recommends magnetic determination techniques based on attractive force and magnetic permeability. Its standardization (AWS A4.2 and ISO 8249) has greatly contributed to the reduction of disagreements between laboratories. Moreover, these techniques are quick, nondestructive, and can be used in laboratories, on-site, or in fabrication lines for quality control. All the details related to the standardization, calibration, and description of the primary and secondary standards can be found in detail in Refs. 5, 7, 9, 17, 22, 23, and 54. Essentially, the method is based on the magnetic response of the δ-ferrite phase as against the nonmagnetic γ-austenite phase.

The techniques employed by different commercial equipment differ in the specific magnetic parameters used to correlate the magnetism with the level of δ-ferrite. The main magnetic techniques currently in use are based on the attractive force (such as Magne-Gage magnetic balance) and on the magnetic permeability (Fischer Feritscope equipment), while some earlier techniques were based on magnetic saturation and the Mössbauer effect.

The technique based on magnetic saturation allowed the determination of % vol of δ-ferrite in the sample, but the intensity of magnetic saturation depends on the chemical composition of the δ-ferrite, which is not easy to determine. Moreover, the technique was destructive and needed the sample to be machined into a precise cylinder.

The attractive force technique is based on the force required to separate the ferromagnetic sample from a standardized permanent magnet in the equipment. The measurement of this force was correlated to the FN scale using calibration standards. The classic example of this equipment (Magne-Gage) is generally considered the reference tool of its type.

The magnetic permeability technique is based on placing a probe coil on the sample that produces a low-frequency electric field, which interacts with the δ-ferrite to generate a magnetic field. The voltage induced by this magnetic field in a separate pickup coil on the probe is proportional to the magnetic permeability and therefore is a direct function of the δ-ferrite content. This technique uses calibration standards. The approximate volume the probe analyzes is around 10 mm^3, and some practical limitations need to be considered:

- The technique requires minimum dimensions of the sample and a minimum distance from the probe to the edge of the sample. These minimum dimensions depend on the specific equipment used. Using the technique with undersized samples or placing the probe near the edge of the sample causes a drop in the measured FN values. The latter is known as edge effect.
- When highly ferromagnetic materials are close to the measurement point, for example in cases of stainless steel claddings on carbon steel plates, it is also necessary to exceed a minimum distance from the probe to the highly ferromagnetic material. If not, overestimation of the Ferrite Number will occur.
- Measurements need to be done on flat surfaces so that the probe contacts perpendicularly on the sample. Regarding the degree of roughness, results obtained from some WRC round-robins

(Refs. 55, 56) showed surface finishing (as-welded, polished, and ground) is a significant variable that influences the FN reading by around ± 10–12%, but it was not possible to establish a consistent trend.

As the δ-ferrite distribution is not homogeneous in the weld metal, it is necessary to ensure a suitable number of readings throughout the sample in order to get an accurate and representative FN value.

Metallographic Determination

Metallographic determination consists of doing a visual quantitative counting — manually or automatically — of the number of subdivisions where the presence of δ-ferrite is detected in a previously polished and metallographically etched sample.

This method is based on the internationally accepted assumption that the ferrite volumetric proportion is analogous to the proportion at the surface measured. The %-vol of δ-ferrite is an arbitrary value that depends on different factors or inherent error sources in the method, like the reagent selection, the operator's ability to distinguish the δ-ferrite from other phases or precipitates, such as carbides, sulphides, σ-phase, the settings and adjustments in contrast if the measurement is done automatically, the measurement procedure (magnification), the counting rules and the statistical coverage to ensure a representative number and distance between points. All these provoke wide dispersion of results between laboratories.

As has been stated, the δ-ferrite distribution is not homogeneous in the weld deposits; therefore, it is first necessary to check that the selected area is microstructurally representative of the whole sample. Other inconveniences are the difficulty in determining with accuracy the counting when the ferrite morphology is too thin, such as in cases of eutectic or skeletal ferrite morphologies.

Since 1976, the ASTM E562 (Ref. 57) standard, which was revised in 2008, has described the procedure for systematic manual point counting and for the statistical estimation of the volume (%) of a microstructurally identified phase. This point counting can be considered valid for the δ-ferrite determination in castings where size and morphology of the ferrite phase is coarser, but it is not recommended for weld metals due to the irregular and thin morphology of the δ-ferrite.

A suitable field of application for quantitative metallography is the determination of the δ-ferrite in the heat-affected zone (HAZ) of duplex welds, as this is so narrow that magnetic measurements do not give accurate results due to the influence of contiguous materials. In this sense, TWI (The Welding Institute) established in 1993 (Ref. 58) some practical recommendations for point counting of the duplex.

Other Minority Methods: X-Ray Diffraction, Electrochemistry, and VSM

This final section shows some minority methods that have been found in the literature.

X-ray Diffraction. The technique is based on exposure of the stainless steel sample to a monochromatic X-radiation and, depending on the crystallographic structure of the phases present (BCC ferrite, FCC austenite), there will be reflection peaks for each phase whose intensity will be related to the concentration of each phase in the sample.

According to the literature (Refs. 7, 10, 16, 19, 59), the quantitative determination of δ-ferrite in stainless steel welds has not been satisfactory, possibly because the fine skeletal morphology of the δ-ferrite and the compositional segregations between the dendrite core and the matrix make the diffraction patterns diffuse. The equipment is expensive and it has only been used in laboratory studies.

Electrochemical Determination. This technique was proposed by Gill et al. (Ref. 60) in 1979. It is based on dissolving the γ-austenite phase and keeping the δ-ferrite phase passivated by exposing it to an electrolyte and a predetermined voltage; therefore, the selective dissolution of the austenite isolates the δ-ferrite, which can be gravimetrically determined.

The limitations and inconveniences are related to the fact that this is a destructive technique, and that it is necessary first to establish the austenite polarization diagram for each alloy where the technique is applied, because the correct voltage is required to ensure the total dissolution of the austenite. It is also an extremely slow method, as it is said to take 40 hours to dissolve the austenite in a 1-mm-thick sample with 3%-vol ferrite.

Magnetometer with Sample Vibration (VSM). This technique was used by Elmer and Eagar in 1990 (Ref. 61) to measure the δ-ferrite content in very small weld samples of mass 5 mg and less than 0.5 mm thickness from EBW and LBW stainless steels (cooled at around 10^4–10^5 °C/s). The small dimensions of the samples would not allow a magnetic measurement or quantitative metallography; therefore, the authors used a magnetometer with sample vibration and a technique based on saturation magnetization of the ferrite.

Conclusions

Determination of δ-ferrite content in stainless steel weld deposits is a topic that has generated much interest and challenged researchers from the early days of welding until today, which is the reason for the development of such a variety of predictive and measurement methods since 1920. Despite their practical limitations, wherever it is possible, experimental measurements based on magnetic determination are better than predictive methods, whose accuracy is mainly dependant on the reliability of chemical composition. However, in those cases where the weld deposit is not available such as in the early stage of projects where alternative welding consumables are being considered, or simply when it is necessary only to get an approximate value, then predictive methods such as WRC-1992, FNN-1999, and the recently presented model for austenitics (Equation 15) have their scope.

Acknowledgments

The author gratefully acknowledges the support of Metrode Products Ltd. and is especially indebted to Dr. Zhuyao Zhang and Adam W. Marshall. The current research is part of the doctoral degree thesis titled "Modelization of δ-ferrite content (FN) in austenitic stainless steels under electric arc conditions," which was submitted for the degree of Doctor in Chemistry by the author at the University of Barcelona, June 29, 2010. The supervision of Dr. Pere Molera and Dr. Núria Llorca from the Department of Materials Science and Metallurgical Engineering at the University of Barcelona is also gratefully acknowledged.

References

1. Brouwer, G. 1978. Ferrite in austenitic stainless steel weld metal — Advantage or disadvantage? *Philips Welding Reporter* (3): 16–19.

2. Lefebvre, J. 1993. Guidance on specifications of ferrite in stainless steel weld metal. *Welding in the World* 31(6): 390–406.

3. Lippold, J. C., and Savage, W. F. 1980. Solidification of austenitic stainless steel weldments: Part II — The effect of alloy composition on ferrite morphology. *Welding Journal* 59(2): 48-s to 58-s.

4. David, S. A. 1981. Ferrite morphology and variations in ferrite content in austenitic stainless steel welds. *Welding Journal* 60(4): 63-s to 71-s.

5. DIN 32514-part 1. 1990. *Determination of Ferrite Number of austenitic weld metal-measurement method.* Düsseldorf, Germany.

6. Prasad Rao, K., and Prasannakumar, S. 1984. Assessment criterion for variability of delta ferrite in austenitic weld and clad metals. *Welding Journal* 63(7): 231-s to 236-s.

7. Stalmasek, E. 1986. Measurement of ferrite content in austenitic stainless steel weld metal giving internationally reproducible results. *WRC Bulletin* (318): 23–98.

8. Kotecki, D. J. 1998. Predicted and measured FN in specifications — A position statement of the experts of IIW Commission IX. Document IIS/IIW-1420-98. *International Institute of Welding.* 5 pages.

9. Kotecki, D. J. 1997. Ferrite determination in stainless steel welds — Advances since 1974. *Welding Journal* 76(1): 24-s to 37-s.

10. Lundin, C. D., Ruprecht, W., and Zhou, G. 1999. Ferrite measurement in austenitic and duplex stainless steel castings. Literature review submitted to SFSA/CMC/DOE. Materials Joining Research Group. University of Tennessee, Knoxville: 40 pages.

11. Olson, D. L. 1985. Prediction of austenitic weld metal microstructure and properties. *Welding Journal* 64(10): 281-s to 295-s.

12. Schaeffler, A. L. 1948. Welding dissimilar metals with stainless electrodes. *Iron Age*. Vol. 162, p. 72.

13. Schaeffler, A. L. 1949. Constitution diagram for stainless steel weld metal. *Metal Progress*. 56(11): 680–680B.

14. DeLong, W. T. 1960. A modified phase diagram for stainless steel weld metals. *Metal Progress.* 77(2): 99–100B.

15. Long, C. J., and DeLong, W. T. 1973. The ferrite content of austenitic stainless steel weld metal. *Welding Journal* 52(7): 281-s to 297-s.

16. DeLong, W. T. 1974. Ferrite in austenitic stainless steel weld metal. *Welding Journal* 53(7): 273-s to 286-s.

17. Reid, H. F., and DeLong, W. T. 1973. Making sense out of ferrite requirements in welding stainless steels. *Metal Progress.* (6): 73–77.

18. Potak, Y. M., and Sagalevich, E. A. 1972. Structural diagram for stainless steels as applied to cast metal and metal deposited during welding. *Avt. Svarka* (5): 10–13.

19. SCRATA. 1981. The measurement of delta ferrite in cast austenitic stainless steels. *Technical bulletin of the Steel Castings Research and Trade Association.* (23), 4 pages.

20. ASTM A800/A800M-91, *Standard practice for steel casting, austenitic alloy, estimating ferrite content thereof.* West Conshohocken, Pa.: ASTM.

21. Björkroth, J., and Henrikson, S. 1965. Ferrite-a structure element with favourable and harmful effects in austenitic stainless welds. *Conference organized by the Swedish Welding Society,* November 23, 1965. 27 pages.

22. ANSI/AWS A4.2-91, *Standard procedures for calibrating magnetic instruments to measure the delta ferrite content of austenitic and duplex austenitic-ferritic stainless steel weld metal.* 1991. Miami, Fla.: American Welding Society.

23. ISO 8249, *Welding. Determination of Ferrite Number (FN) in austenitic and duplex ferritic-austenitic Cr-Ni stainless steel weld metals.* 2000. Brussels, Belgium: ISO.

24. Hull, F. C. 1973. Delta ferrite and martensite formation in stainless steels. *Welding Journal* 51(5): 193-s to 203-s.

25. Kotecki, D. J., and Szumachowski, E. R. 1983. Manganese effect on stainless steel weld metal ferrite. IIW Document II-C-706-83. *IIW International Institute of Welding.* 26 pages.

26. Kotecki, D. J. 1986. Silicon effect on stainless steel weld metal ferrite. *IIW International Institute of Welding.* Doc. reference II-C-779-86. 7 pages.

27. Kotecki, D. J. 1983. Molybdenum effect on stainless steel weld metal ferrite. *IIW International Institute of Welding.* Document reference II-C-707-83. 6 pages.

28. Kotecki, D. J. 1982. Extension of the WRC Ferrite Number system. *Welding Journal* 61(11): 352-s to 361-s.

29. Kotecki, D. J. 1986. Ferrite control in duplex stainless steel weld metal. *Welding Journal* 65(10): 273-s to 278-s.

30. Siewert, T. A., McCowan, C. N., and Olson, D. L. 1988. Ferrite Number prediction to 100 FN in stainless steel weld metal. *Welding Journal* 67(12): 289-s to 298-s.

31. McCowan, C. N., Siewert, T. A., and Olson, D. L. 1989. Stainless steel weld metal: Prediction of ferrite content. *WRC Bulletin* (342), 36 pages.

32. Kotecki, D. J., and Siewert, T. A. 1992. WRC-1992 Constitution Diagram for stainless steel weld metals: A modification of the WRC-1988 Diagram. *Welding Journal* 71(5): 171-s to 178-s.

33. Feldstein, J. 1993. The WRC Diagram. *Svetsaren.* 47(2): 36–39.

34. Kotecki, D. J. 1999. A martensite boundary on the WRC-1992 diagram. *Welding Journal* 78(5): 181-s to 192-s.

35. Kotecki, D. J. 1999. Martensite prediction in stainless steel weld cladding. *Paper presented at the Stainless Steel World Conference* (2): 573–583.

36. Balmforth, M. C., and Lippold, J. C. 2000. A new ferritic-martensitic stainless steel constitution diagram. *Welding Journal* 79(12): 339-s to 345-s.

37. Aström, H. 1998. Prediction of FN from chemical analysis. ELGA technical memo. 6 pages.

38. Kannan, T., and Murugan, N. 2006. Prediction of Ferrite Number of duplex stainless steel clad metals using RSM. *Welding Journal* 85(5): 91-s to 100-s.

39. Anderson, T., Perricone, M. J., DuPont, J. N., and Marder, A. R. 2007. The influence of molybdenum on stainless steel weld microstructures. *Welding Journal* 86(9): 281-s to 292-s.

40. Bhadeshia, H. K. D. H., and Stone, H. J. 2009. *ASM Handbook: Fundamentals of Modeling for Metals Processing.* Neural-network modeling. Volume 22A: 435–439. Materials Park, Ohio: ASM International.

41. Vasudevan, M., Murugananth, M., and Bhaduri, A. K. 2002. Application of Bayesian neural network for modeling and prediction of Ferrite Number in austenitic stainless steel welds. *Mathematical Modelling of Weld Phenomena 6.* Ed. H. Cerjak. Maney Publishing.

42. Vitek, J. M., Iskander, Y. S., and Oblow, E. M. 2000. Improved Ferrite Number prediction in stainless steel arc welds using artificial neural networks — Part 1: Neural network development. *Welding Journal* 79(2): 33-s to 40-s.

43. Vitek, J. M., Iskander, Y. S., and Oblow, E. M. 2000. Improved Ferrite Number prediction in stainless steel arc welds using artificial neural networks — Part 2: Neural network results. *Welding Journal* 79(2): 41-s to 50-s.

44. Vitek, J. M., David, S. A., and Hinman, C. R. 2003. Improved Ferrite Number prediction model that accounts for cooling rate effects — Part 1: Model development. *Welding Journal* 82(1): 10-s to 17-s.

45. Vitek, J. M., David, S. A., and Hinman, C. R. 2003. Improved Ferrite Number prediction model that accounts for cooling rate effects — Part 2: Model results. *Welding Journal* 82(2): 43-s to 50-s.

46. Valiente Bermejo, M. A. 2010. *Modelization of δ-ferrite content (FN) in austenitic stainless steels under electric arc conditions.* PhD dissertation. University of Barcelona. ISBN 978-84-693-5713-2.

47. Valiente Bermejo, M. A. 2011. Modelization of δ-ferrite content in austenitic stainless steel weld metals. IIW Document IX-2358-11. *64th Annual Assembly of the International Institute of Welding.* July 17–20. Chennai, India. 20 pages.

48. Hammar, Ö., and Svensson, U. 1979. Influence of steel composition on segregation and microstructure during solidification of austenitic stainless steels. *International Conference on Solidification and Casting of Metals.* Sheffield, UK. The Metals Society, pp. 401–410.

49. Elmer, J. W., Allen, S. M., and Eagar, T. W. 1989. The influence of cooling rate on the ferrite content of stainless steel alloys. *Proceedings of the 2nd International Conference on Trends in Welding Research*, May 14–18, 1989. Gatlinburg, Tenn.: ASM International, pp. 165–170.

50. Katayama, S., and Matsunawa, A. 1984. Solidification microstructure of laser welded stainless steels. *Proceedings International Congress on Applications of Lasers & Electro-Optics (ICALEO).* Laser Institute of America 44: 60–67.

51. Lippold, J. C. 1994. Solidification behavior and cracking susceptibility of pulsed-laser welds in austenitic stainless steels. *Welding Journal* 73(6): 129-s to 139-s.

52. David, S. A., Vitek, J. M., and Hebble, T. L. 1987. Effect of rapid solidification on stainless steel weld metal microstructures and its implications on the Schaeffler diagram. *Welding Journal* 66(10): 289-s to 300-s.

53. Johnson, E., Grabaek, L., Johansen, A., Sarholt Kristensen, L., and Wood, J. V. 1988. Microstructure of rapidly solidified stainless steel. *Materials Science and Engineering* 98(2): 301–303.

54. McCowan, C. N., Siewert, T. A., Vigliotti, D. P., and Wang, C. M. 2001. Reference materials for weld metal ferrite content: Gauge calibration and material characterization. *Welding Journal* 80(4): 106-s to 114-s.

55. Siewert, T. A, Siewert, E. A., Farrar, J. C. M., and Zhang, Z. 2002. Statistical evaluation of a round-robin experiment: Uncertainties in ferrite measurement in weldments. IIW Document IX-H-531-02. *International Institute of Welding Commission IX.* 23 pages.

56. Farrar, J. C. M. 2004. The Measurement of Ferrite Number (FN) in Real Weldments — Final Report. IIW Document IX-H-590-04. *International Institute of Welding. Commission IX.* 16 pages.

57. ASTM E562-83, *Standard practice for determining volume fraction by systematic manual point count*. 1984. West Conshohocken, Pa.: ASTM.

58. TWI. 1993. *Recommended practice for determining volume fraction of ferrite in duplex stainless steel weldments by systematic point count.* Ref. 5632/18/93. Six pages.

59. Bonnet, C., Lethuillier, P., and Rouault, P. 2000. Comparison between different ways of ferrite measurements in duplex welds and influence on control reliability during construction. *Duplex America 2000 Conference*, pp. 431–442.

60. Gill, T. P. S., Dayal, R. K., and Gnanamoorthy, J. B. 1979. Estimation of delta ferrite in austenitic stainless steel weldments by an electrochemical technique. *Welding Journal* (12): 375-s to 378-s.

61. Elmer, J. W., and Eagar, T. W. 1990. Measuring the residual ferrite content of rapidly solidified stainless steel alloys. *Welding Journal* 64(4): 141-s to 150-s.